Virtual Power Angle Synchronous Control for Improving Transient Stability of Grid-forming Converters

Jidong Xu, Jun Zeng, Gengning Ying, Minhai Wu, and Junfeng Liu

***Abstract*—The increasing adoption of grid-forming converters (GFMCs) stems from their capacity to furnish voltage and frequency support for power grids. Nevertheless, GFMCs employing the current reference saturation limiting method often exhibit instability during various transient disturbances including grid voltage sags, frequency variations, and phase jumps. To address this problem, this paper proposes a virtual power angle synchronous (δ_v-SYN) control method. The fundamental of this method is to achieve synchronization with the grid using the virtual power angle δ_v instead of the active power. The transient stability characteristics of the proposed method are theoretically elucidated using a novel virtual power angle-power angle (δ_v-δ) model. The key benefit of the proposed method is its robustness to various grid strengths and diverse forms of transient disturbances, eliminating the requirement for fault identification or control switching. Moreover, it can offer grid-forming support to the grid during grid faults. Hardware-in-the-loop experimental results validate the theoretical analysis and the performance of the proposed method.**

***Index Terms*—Grid-forming converter, inertial effect, overcurrent limitation, transient disturbance, transient stability, virtual synchronous control.**

I. Introduction

As renewable energy sources and energy storage systems continue to increase rapidly, the traditional electric power systems based on synchronous generators (SGs) are gradually transitioning towards the dominance of converter-interfaced generators such as converters utilized in solar generation and wind turbines [1], [2]. It is crucial for the power grid to operate these converters in the grid-forming mode, providing essential functions like frequency and voltage support, which is provided by SGs in conventional grids. Till now, there have been many studies on grid-forming converters (GFMCs). Research has been conducted in the analysis and improvement of small-signal synchronization stability of GFMCs [3]-[5].

To ensure the stability of the power grid, the GFMCs should also maintain grid synchronization under various transient disturbances such as voltage sags, frequency variations, and phase jumps. Furthermore, the GFMCs should automatically return to normal operation when the fault is cleared. In the power grid, this capability is referred to as transient stability. The transient stability of GFMCs has been much discussed [6]-[10]. The analysis in [6]-[8] investigated how inertia affects the transient stability of the GFMC and demonstrated that inertia adversely affects transient stability. The impact of the internal voltage on the transient stability is studied in [9]. In [10], the impact of the feedback modes of the power synchronous control on the transient stability of the GFMC is detected. However, these analyses fail to account for the influence of current saturation on transient stability.

Limiting the output current of GFMCs within the safe range is crucial. Different from SGs, which have large overcurrent capability, the overcurrent capability of GFMCs is very limited, i.e., 1.2 p.u. [11]. Without proper control, transient disturbances can cause overcurrent in the GFMC, thus damaging power electronic switches. Existing literature has proposed several methods to limit the output current of the GFMC to the allowable value. The first is the current reference saturation (CRS) limiting method [12]-[14]. The second is the virtual impedance current limitation method [15]-[17]. However, the effectiveness of the second method is affected by variations in grid impedance and cannot precisely limit the current. As shown in [18], an overcurrent phenomenon occurs during the early stages of the grid voltage sags with the second method. The CRS limiting method is widely used due to its rapid and precise current-limiting capability. Therefore, this paper adopts the CRS limiting method for the current limitation.

Reference [19] reveals that GFMCs experience transient instability under voltage sag conditions and it has been highlighted that the CRS limiting method has a considerable negative influence on the transient stability of GFMCs. Numer-

Manuscript received: June 28, 2024; revised: September 23, 2024; accepted: November 14, 2024. Date of CrossCheck: November 14, 2024. Date of online publication: January 30, 2025.

This work was supported in part by the National Natural Science Foundation of China (No. 52377186), the Natural Science Foundation of Guangdong Province (No. 2024A1515012428), the Science and Technology Planning Project of Guangdong Province, China (No. 2023A1111120023), and the Basic and Applied Basic Research Foundation of Guangdong Province (No. 2022A1515240026).

J. Xu, J. Zeng, G. Ying, and M. Wu are with the School of Electric Power Engineering, South China University of Technology, Guangzhou 510640, China (e-mail: 202221014917@mail.scut.edu.cn; junzeng@scut.edu.cn; 202110182778@mail.scut.edu.cn; minhaiwu@foxmail.com).

J. Liu (corresponding author) is with the School of Automation Science and Engineering, South China University of Technology, Guangzhou 510641, China (e-mail: jf.liu@connect.polyu.hk).

DOI: 10.35833/MPCE.2024.000684

ous control techniques have been proposed to enhance the system transient stability of GFMCs involving the CRS limiting method under voltage sag conditions. A stability enhanced *P-f* droop control (SEPFC) is introduced in [19]. The SEPFC adds the filter capacitor voltage into the droop control to improve the transient stability. However, the study points out that this method fails under weak grid conditions. Reference [20] indicates that during voltage sags, active power synchronous (P-SYN) control can be switched to reactive power synchronous (Q-SYN) control to prevent desynchronization from the power grid. However, this method requires the grid impedance measurements, which can be quite difficult to obtain. A power angle-frequency droop control is proposed in [21], which establishes steady-state operating points under fault conditions to avoid transient instability. However, this method fails under weak grid or severe voltage drop conditions. The aforementioned methods ignore the impact of inertia, enhancing the transient stability of GFMCs effectively only during voltage sags, but proving ineffective for other transient disturbances. The frequency variation and phase jump cases are common in the grid with higher renewable energy penetration and lower inertia, which might cause power grid instability as well.

Reference [22] further analyzes the instability mechanism of GFMCs under phase jump conditions. The authors address this instability problem by modifying the saturation current phase reference, but the parameter design procedure of this method is complex and difficult to implement. Reference [23] analyzes the instability mechanism of GFMCs under frequency variation conditions and presents an overcurrent limitation scheme based on power angle. However, it is unsuitable for implementation in weak grid scenarios, and the recovery time after the fault is prolonged.

A detailed analysis of the instability mechanisms of GFMCs with P-SYN control and the CRS limiting method under various transient disturbances is carried out in this paper. Based on this, this paper suggests a virtual power angle synchronous (δ_v-SYN) control method. The fundamental of this method is to achieve synchronization with the grid using virtual power angle δ_v instead of active power. This method ensures the presence of a steady-state equilibrium point even during serious transient disturbances, which significantly improves the transient stability of GFMCs. The virtual power angle-power angle (δ_v-δ) model is developed for both voltage source mode (VSM) and current source mode (CSM), which enables a theoretical interpretation of the transient stability of the proposed method. Moreover, the benefits of the proposed method are as follows.

1) This method is robust to different grid strengths, ranging from very weak to strong grids, and can effectively handle various transient disturbances such as grid voltage sags, frequency variations, and phase jumps.

2) This method ensures a smooth switching between normal operation and fault operation without the need for fault diagnosis.

3) This method can offer voltage and frequency support to the grid during transient disturbances.

The rest of this paper is organized as follows. Section II provides the configuration of the studied system and the phasor-based model for transient stability analysis. Section III analyzes the transient stability of the GFMC with the P-SYN control and the CRS limiting method, demonstrating that the GFMC loses synchronization with the power grid during grid voltage sags, frequency variations, and phase jumps. Section IV introduces the proposed δ_v-SYN control method. A δ_v-δ model for transient stability analysis is also established. The analysis of the impact of the proposed method on the transient stability of the GFMC is conducted using the δ_v-δ model. Section V analyzes the dynamic performance and robustness of the proposed method under various grid strengths through time-domain simulations. And a comparison between the proposed method and existing state-of-the-art solutions is conducted. Section VI confirms the theoretical analysis and performance of the proposed method by hardware-in-the-loop (HIL) experiments. Finally, Section VII provides the conclusion for this paper.

II. Configuration of Studied System and Phasor-based Model for Transient Stability Analysis

A. Configuration of Studied System

Figure 1(a) depicts the configuration of a GFMC connected to the power grid, where PWM stands for pulse width modulation; v_{gabc} represents the grid voltage; v_{abc} represents the output voltage at the point of common coupling (PCC); i_{Labc} represents the converter-side current; i_{abc} represents the grid-side current; and L_g represents the line inductance. Additionally, in this paper, the converter uses the LC filter, where L_f and C_f represent the filter inductance and capacitance, respectively. The LCL filter can also be used to filter out harmonics. Since the grid-side inductance of the LCL filter is generally small and can be considered part of the line inductance, the proposed method can also be applied to converters using an LCL filter, and the theoretical analysis presented in this paper is still valid.

Outer loop control includes an active power controller (APC) and a reactive power controller (RPC). Inner loop control includes a voltage controller (VC) with virtual admittance and a current-limiting controller (CLC). The phase reference θ_{ref} for Park transformation is obtained from the APC, in which droop control along with inertial and damping emulation is integrated [24]. P_{ref} represents the reference value of active power. P represents the active power output of the converter. P_m represents the set value of active power. ω_n represents the nominal angular frequency. K_p represents the virtual damping. H represents the inertia constant. D represents the droop coefficient. $\Delta\omega$ represents the angular frequency increment. ω represents the output angular frequency of APC. RPC employs reactive power-voltage droop control to derive the voltage reference E_{ref}. n_q represents the droop coefficient of RPC control. Q_{ref} represents the reference value of reactive power. Q represents the reactive power output of the converter. V_N represents the voltage amplitude setting value. *LPF* denotes a first-order low-pass filter (LPF) utilized for filtering out harmonics from reactive power. θ_{ref} and E_{ref} produce the references $e_{\alpha\beta}$ used by the VC with vir-

tual admittance. $v_{\alpha\beta}$ represents the PCC voltage in the $\alpha\beta$ coordinate system. The VC incorporates virtual inductance L_v and virtual resistance R_v. To get precise and decoupled control of the APC and RPC, R_v is set significantly lower than L_v [25]. Hence, the virtual resistance is ignored in this paper. The output of the VC with virtual admittance is $i_{L\alpha\beta}^{ref}$, which is the converter-side current reference in the $\alpha\beta$ coordinate system.

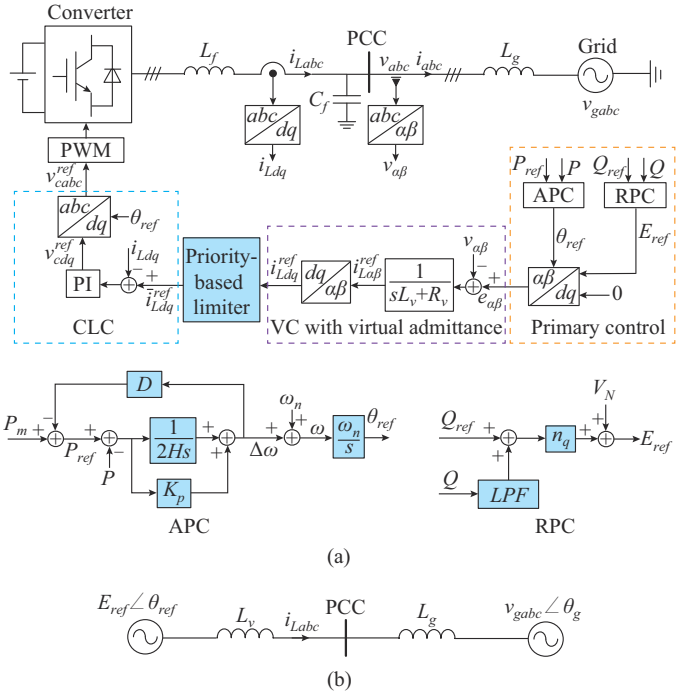

Fig. 1. Schematic illustration of GFMC incorporating P-SYN control and CRS limiting method. (a) Configuration and control. (b) Equivalent circuit.

The CLC incorporates a current reference limiting strategy and regulates the converter-side current i_{Ldq}, utilizing the proportional-integral (PI) decoupled dq control method. The output of the CLC is v_{cdq}^{ref}, which is the terminal voltage reference of the converter in the dq coordinate system. v_{cdq}^{ref} undergoes the transformation from the dq coordinate system to the abc coordinate system, resulting in the three-phase terminal voltage reference v_{cabc}^{ref}. The widely adopted d-axis-priority CRS limiting method is selected to control the output of the VC [11]. This limiting method is defined using (1) and (2), with the maximum current typically set to be 1.2 p.u., denoted as $I_{\max}$.

$$\bar{i}_{Ld}^{ref}=\frac{i_{Ld}^{ref}}{\left|i_{Ld}^{ref}\right|}\min\left(\left|i_{Ld}^{ref}\right|,I_{\max}\right) \tag{1}$$

$$\bar{i}_{Lq}^{ref}=\frac{i_{Lq}^{ref}}{\left|i_{Lq}^{ref}\right|}\min\left(\left|i_{Lq}^{ref}\right|,\sqrt{I_{\max}^2-(\bar{i}_{Ld}^{ref})^2}\right) \tag{2}$$

where i_{Ld}^{ref} and i_{Lq}^{ref} are the converter-side current references produced through the VC in the dq coordinate system; and $\bar{i}_{Ld}^{ref}$ and $\bar{i}_{Lq}^{ref}$ are the saturated current references.

From (1) and (2), if the current magnitude is below $I_{\max}$, the CRS limiting method remains inactive and the GFMC exhibits characteristics similar to a voltage source. Conversely, if the current magnitude exceeds $I_{\max}$, the CRS limiting method is activated. Under these circumstances, the current magnitude is constrained to $I_{\max}$. Its phase is aligned with the d axis. Besides, Fig. 1(b) illustrates the equivalent circuit of the studied system under the voltage source operation characteristics, where θ_g represents the phase of the grid voltage.

B. Phasor-based Model for Transient Stability Analysis

Typically, the inner control loop exhibits dynamics that are more than ten times faster than those of the outer control loop [26]. When analyzing the transient stability problem arising from the P-SYN control, the faster response speed of the inner control loop allows it to be ignored. The current of the capacitor C_f is also ignored, as the capacitor primarily filters the harmonics of the current and has minimal influence on the transient stability in this paper. In power transmission scenarios, the line resistance R_g relative to the line reactance X_g is ignored due to $R_g \ll X_g$. Then, phasor-based models are derived utilizing these assumptions. The HIL experiments in this study will comprehensively consider all factors ignored in the assumptions to ensure the validity of the analysis and the efficacy of the proposed method.

The power angle δ represents the phase disparity between the phase reference θ_{ref} and the grid voltage phase θ_g.

$$\delta=\theta_{ref}-\theta_g=\int(\omega-\omega_n)\mathrm{d}t \tag{3}$$

As depicted in Fig. 2(a), when the CRS limiting method remains inactive, the GFMC terminal voltage $\vec{E}$ is regulated to align with the d axis, where $\vec{Z}_v=\mathrm{j}\omega_n L_v$ and $\vec{Z}_g=\mathrm{j}\omega_n L_g$ represent the virtual impedance and line impedance, respectively. $\vec{I}_{\max}$ represents the maximum current phasor. $\vec{I}_g$ and $\vec{V}_g$ represent the voltage and current phasors of the grid, respectively. $\vec{V}_{pcc}$ represents the PCC voltage phasor. The virtual power angle δ_v is defined as the phase difference between $\vec{E}$ and $\vec{V}_{pcc}$.

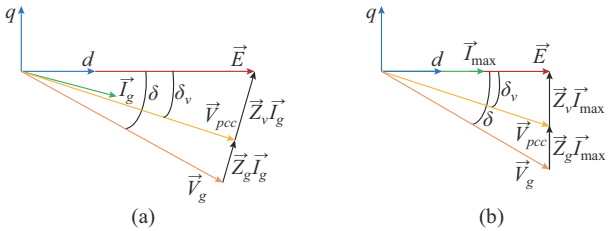

Fig. 2. Phasor diagrams of different modes. (a) VSM. (b) CSM.

In this scenario, the P-δ equation is described as:

$$P=\frac{3}{2}\frac{EV_g}{X_v+X_g}\sin(\delta) \tag{4}$$

where E and V_g represent the magnitudes of $\vec{E}$ and $\vec{V}_g$, respectively; and X_v represents the virtual reactance.

It is noteworthy that the filter inductance L_f is not ignored, but is replaced with a virtual inductance larger than that in (4). From the perspective of the physical significance of virtual admittance control, L_v represents the equivalent inductance between the terminal voltage of the converter and the PCC voltage, which corresponds to L_f in the actual circuit to-

pology, as shown in the equivalent circuit of the system in Fig. 1(b). According to [27], to ensure the small-signal stability of the converter, the virtual inductance must be greater than 0.4 p.u.. Based on the filtering performance and cost, L_f is set to be 0.2 p.u.. Therefore, the virtual admittance method does not neglect L_f but actually increases it. Since L_f is replaced with a larger virtual inductance, it will not affect the power angle equation (4). Besides, the parameter of L_v should not be too large either. This is because the virtual inductance and virtual resistance create an LPF in the control path, and an excessively large L_v will reduce the bandwidth of the filter, thereby decreasing the dynamic performance of the system. Based on the above analysis, the virtual inductance is set to be 0.8 p.u..

Furthermore, as depicted in Fig. 2(b), when the CRS limiting method is activated, the VC becomes ineffective due to current saturation, causing the GFMC to work as a current source. Thus, the GFMC changes from VSM to CSM after a grid fault. The output current $\vec{I}_{\max}$ is regulated to align with the d axis. Thus, the output power of the GFMC can be calculated using $\vec{I}_{\max}$ and $\vec{V}_g$. In this scenario, the output power P can be reformulated as:

$$P = \frac{3}{2} I_{\max} V_g \cos(\delta) \tag{5}$$

III. Transient Stability Analysis of GFMCs with P-SYN Control and CRS Limiting Method

This section describes the transient stability characteristics of GFMCs with the P-SYN control and CRS limiting method during various transient disturbances.

A. Transient Instability of P-SYN Control in Case of Voltage Sags

The transient stability of GFMCs with the P-SYN control and CRS limiting method under voltage sags is analyzed in this subsection. The analysis employs the P-δ curves for both VSM and CSM. The focus is on assessing the existence of stable equilibrium points under transient disturbances.

Based on the APC in Fig. 1 and (3), we can obtain:

$$\dot{\delta} = \omega - \omega_n = (P_{ref} - P)\left(\frac{1}{2Hs} + K_p\right) \tag{6}$$

The operational mechanism of the GFMC under a voltage sag is depicted in Fig. 3, which illustrates the P-δ curves based on (4) and (5). As shown in Fig. 3, the GFMC with the P-SYN control and CRS limiting method can restore synchronization with the grid following the sequence of a → b → c → d → e → a and lose synchronization following the sequence of a → b → c → d → e′.

Under normal conditions, the operating point is stabilized at equilibrium point a, and the output angular frequency of the converter is equal to the rated grid frequency ω_n. δ at point a is defined as δ_a. When V_g suddenly decreases from 311 V (1 p.u.) to 62 V (0.2 p.u.), the CRS limiting method will promptly be activated, yet δ will not undergo an abrupt change.

Consequently, the operating point will jump from the standard/post-fault curve under VSM to the fault curve under CSM. Because $P_{ref} > P$ on the fault curve under CSM, based on (6), the output angular frequency ω begins to increase, leading to a corresponding rise in δ. Thus, the operating point will move along the fault curve under CSM until V_g returns to its nominal value at point b. δ at point b is defined as the clearing angle δ_c. When V_g returns to its normal value, the operating point jumps from point b to point c. At point c, the output power $P > P_{ref}$. According to (6), the output angular frequency ω begins to decrease, but the angular frequency increment $\Delta\omega = \omega - \omega_n$, which is obtained through the integration of the virtual inertia component during the fault stage, does not immediately return to zero at the moment the fault is cleared. Consequently, the output angular frequency ω is still greater than the grid frequency when the fault is cleared. δ will continue to increase and the operating point will move along the post-fault curve under CSM until ω is less than ω_n. If the operating point does not cross the unstable equilibrium point d when ω decreases to a value smaller than ω_n, due to $P_{ref} < P$, based on (6), δ will decrease and the operating point will move along the post-fault curve under CSM until it reaches point e. After point e, the CRS limiting method will be deactivated. The operating point will transition following the standard/post-fault curve under VSM back to point a. If δ crosses the unstable equilibrium point d, due to $P_{ref} > P$, δ will increase and the operating point will move along the post-fault curve under CSM. This results in the GFMC becoming desynchronized from the grid, which in turn gives rise to transient instability.

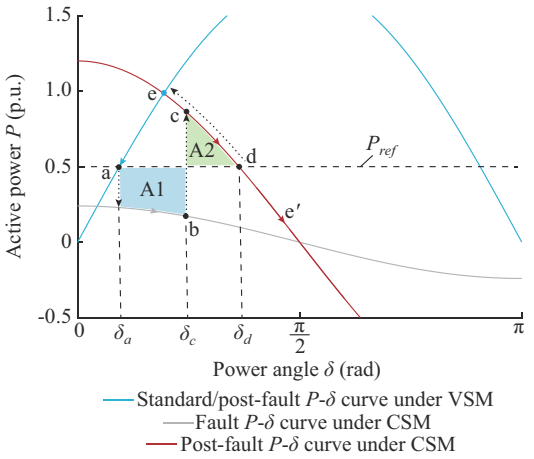

Fig. 3. Operational mechanism of GFMC under a voltage sag.

According to the equal area criterion, a successful fault recovery requires that the acceleration area A1 is smaller than the maximum deceleration area A2. The equal area criterion essentially analyzes the transient stability of GFMCs from the perspective of energy conversion. As the operating point moves from point a to point b, ω increases continuously, accelerating the converter. During a voltage sag, the rotor of SG accelerates, and electrical energy is converted into the kinetic energy of the rotor. The converter undergoes a similar process in which the equivalent potential energy of the converter E_P is converted into the equivalent kinetic energy of the converter E_k during a voltage sag. The increase in E_k can be represented by the acceleration area A1.

$$E_k = E_p = \int_{\delta_a}^{\delta_c} \left(P_{ref} - \frac{3}{2} I_{\max} \cdot 0.2 V_g \cos(\delta) \right) \mathrm{d}\delta \tag{7}$$

where $\delta_a = \arcsin \dfrac{2P_{ref}(X_v + X_g)}{3EV_g}$.

After the fault is cleared, as the operating point moves from point c to point d, the output angular frequency ω begins to decrease, indicating that the equivalent kinetic energy of the converter is being converted into the equivalent potential energy. The maximum convertible equivalent potential energy $E_{p\max}$ is determined by the maximum deceleration area A2, which is given as:

$$E_{p\max} = \int_{\delta_c}^{\delta_d} \left(\frac{3}{2} I_{\max} V_g \cos(\delta) - P_{ref} \right) \mathrm{d}\delta \tag{8}$$

δ at point d is defined as δ_d.

$$\delta_d = \arccos \frac{P_{ref}}{\dfrac{3}{2} I_{\max} V_g} \tag{9}$$

If $E_k < E_{p\max}$, i.e., the acceleration area A1 is smaller than the maximum deceleration area A2, E_k obtained by the converter during the fault can be completely converted into E_p. This results in a reduction in ω, enabling it to return to the grid frequency ω_n before the operating point reaches the unstable equilibrium point d, thereby the further power angle increase is prevented. Based on (6), δ will decrease as ω drops below the grid frequency ω_n. The operating point eventually reaches the steady-state equilibrium point a. If $E_k > E_{p\max}$, ω is still greater than ω_n when the operating point reaches the unstable equilibrium point d. δ will pass beyond the unstable equilibrium point d, resulting in transient instability.

Assume that the acceleration area A1 is equal to A2 when δ_c is equal to the critical clearing angle (CCA) δ_{cc}. Under this condition, δ will approach the unstable equilibrium point d during the dynamic process, but will not exceed it.

δ_{cc} can be determined as:

$$\int_{\delta_a}^{\delta_{cc}} \left(P_{ref} - \frac{3}{2} I_{\max} \cdot 0.2 V_g \cos(\delta) \right) \mathrm{d}\delta = \int_{\delta_{cc}}^{\delta_d} \left(\frac{3}{2} I_{\max} V_g \cos(\delta) - P_{ref} \right) \mathrm{d}\delta \tag{10}$$

$$\delta_{cc} = \arcsin \left(1.25 \sin(\delta_d) - 0.25 \sin(\delta_a) + \frac{P_{ref}(\delta_a - \delta_d)}{1.2 I_{\max} V_g} \right) \tag{11}$$

When δ_c exceeds δ_{cc}, the operating point will pass beyond the unstable equilibrium point d and the system will experience transient instability. Consequently, an extended fault duration and an excessive grid voltage drop during the fault process have the potential to induce transient instability. It is of great importance to prevent this instability, as it has the potential to significantly compromise the secure operation of the system.

B. Transient Instability of P-SYN Control in Case of Frequency Variations

Based on (4) and (5), the operational mechanism of the GFMC under frequency variations is depicted in Fig. 4. At point b, the current magnitude reaches its maximum value $I_{\max}$. δ at the operating point of the current critical saturation is defined as δ_{cv}. As the grid frequency f_g decreases from f_1 of 50 Hz to f_2 of 49.6 Hz, the output power of the converter increases from P_1 to P_2, and the operating point shifts from point a towards point b. Hence, the output current magnitude exceeds $I_{\max}$. To constrain the output current, the CRS limiting method is activated. As f_g decreases from f_1 to f_2, the operating point exceeds the unstable operating point c, and the GFMC becomes desynchronized from the grid. Under this condition, the system is unstable.

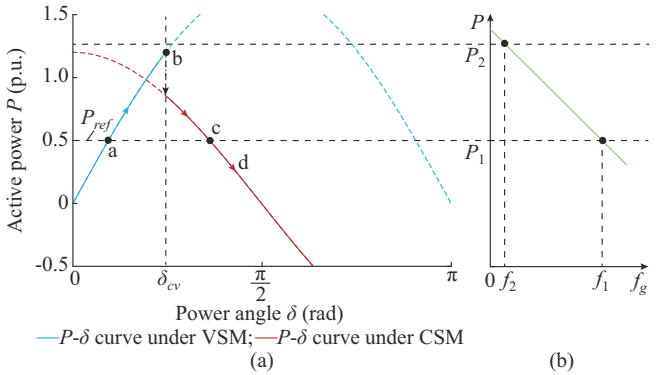

Fig. 4. Operational mechanism of GFMC under frequency variations. (a) P-δ curves. (b) P-f_g curve.

C. Transient Instability of P-SYN Control in Case of Phase Jump

Before delving into the instability mechanism of the phase jump case, we will first explain the concept of the auto-recovery boundary. Within the range of $(-\delta_{cv}, \delta_{cv})$, the GFMC can autonomously exit the CSM and revert to the VSM. When the CSM is activated, it requires the current reference produced by the VC to be less than the maximum current to exit the CSM, i.e.,

$$\left| (E_{ref} \angle \delta - V_g \angle 0) / Z_{total} \right| < I_{\max} \tag{12}$$

where $Z_{total} = \omega_n (L_v + L_g)$.

Considering that both the terminal voltage amplitude reference of the converter E_{ref} and the post-fault voltage amplitude V_g are equal to V_N, the boundary power angle $\pm\delta_{cv}$ for exiting the CSM is derived from (12) as:

$$\delta_{cv} = \arccos \left(1 - \frac{1}{2} \left[\frac{(X_g + X_v) I_{\max}}{V_N} \right]^2 \right) \tag{13}$$

If δ is within the range of $(-\delta_{cv}, \delta_{cv})$, the GFMC will automatically revert to the VSM. If the power angle exceeds the range of $(-\delta_{cv}, \delta_{cv})$, the converter will remain in the CSM before δ returns to the range of $(-\delta_{cv}, \delta_{cv})$.

The operational mechanism of the GFMC under phase jumps of −40° and −60° is depicted in Fig. 5. When a phase jump of −40° occurs, the operating point jumps to point e from point a. Due to $P_{ref} < P$ at point e, based on (6), δ will decrease and the operating point will move along the P-δ curve under CSM until $\delta = \delta_{cv}$ at point b. Then, the CRS limiting method will be deactivated, and the operating point will jump to point b and follow the P-δ curve under VSM back to point a.

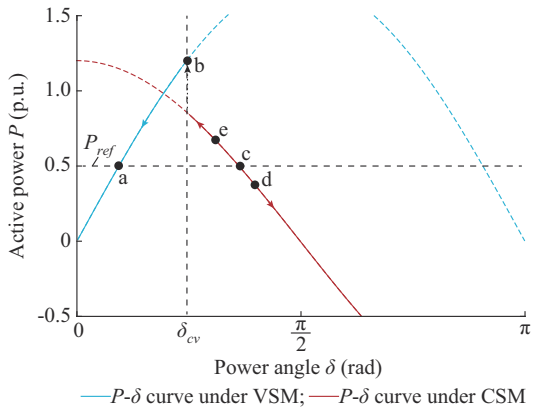

Fig. 5. Operational mechanism of GFMC under phase jump.

For the GFMC with the CRS limiting, when a phase jump of −60° occurs, δ will abruptly increase from point a to point d. As a result, the CSM is triggered, and the operating point crosses the unstable operating point c. Due to $P_{ref} > P$ at point d, according to (6), δ will increase, causing the operating point to move along the P-δ curve under CSM, ultimately leading to unsynchronization between the GFMC and the grid.

IV. Proposed δ_v-SYN Control Method and δ_v-δ Model for Transient Stability Analysis

A. Description of δ_v-SYN Control and δ_v-δ Model

According to the analysis in Section III, the P-SYN control with the CRS limiting method suffers from transient instability problems during transient disturbances. From (4), we can find that the active power is proportional to the power angle. It is therefore possible to consider the direct use of the power angle δ for synchronous control. However, the calculation of δ needs the parameters of the grid voltage and the line impedance, which can be rather challenging. Alternatively, the calculation of δ_v is relatively convenient. According to Fig. 1, the output of the APC is θ_{ref} of $\vec{E}$. The phase of v_{abc} can be obtained by using the phase-locked loop (PLL), which is defined as θ_{pll}. Therefore, δ_v can be obtained as:

$$\delta_v = \theta_{ref} - \theta_{pll} \tag{14}$$

Through (15), we can derive the virtual power angle reference δ_{vref} from the active power reference. Considering that the terminal voltage amplitude of the converter E and the PCC voltage amplitude V_{pcc} are both equal to V_N, we can obtain:

$$P_{ref} = \frac{3}{2}\frac{V_N^2}{X_v}\sin(\delta_{vref}) \tag{15}$$

$$\delta_{vref} = \arcsin\left(\frac{2P_{ref}X_v}{3V_N^2}\right) \tag{16}$$

Once δ_v and δ_{vref} are obtained, the δ_v-SYN control can produce the angular frequency reference of the converter as:

$$\dot{\delta} = \omega - \omega_n = (\delta_{vref} - \delta_v - D\Delta\omega)\left(\frac{1}{2Hs} + K_p\right) \tag{17}$$

Figure 6 depicts a control block diagram of δ_v-SYN control. The transient stability analysis of the δ_v-SYN control relies on the δ_v-δ curves and necessitates an evaluation of the existence of an equilibrium point during transient disturbances.

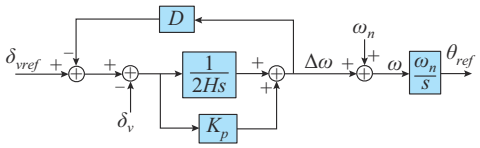

Fig. 6. Control block diagram of δ_v-SYN control .

In steady-state operation, P can be calculated both through δ and δ_v, as illustrated in (18).

$$P = \frac{3}{2}\frac{EV_g}{X_v + X_g}\sin(\delta) = \frac{3}{2}\frac{EV_{pcc}}{X_v}\sin(\delta_v) \tag{18}$$

From (18), the δ_v-δ equation under the VSM can be derived as:

$$\delta_v = \arcsin\left(\frac{V_g X_v}{(X_v + X_g)V_{pcc}}\sin(\delta)\right) \tag{19}$$

From Fig. 2(b), the δ_v-δ equation under the CSM can be derived as:

$$\frac{\tan(\delta_v)}{\tan(\delta)} = \frac{X_v}{X_g + X_v} \tag{20}$$

Then, δ_v under the CSM can be derived from (20) as:

$$\delta_v = \arctan\left(\frac{X_v}{X_v + X_g}\tan(\delta)\right) \tag{21}$$

B. Transient Stability Analysis of δ_v-SYN Control in Case of Voltage Sag

In this subsection, the transient stability of δ_v-SYN control under voltage sags is analyzed utilizing the δ_v-δ equation (19).

First, we investigate the transient stability of δ_v-SYN control under strong grid conditions. Figure 7 shows the δ_v-δ curves and P-δ curves of the GFMC under a voltage sag when the short circuit ratio (SCR) is 15. During the voltage sag, the grid voltage magnitude decreases from 311 V (1 p.u.) to 62 V (0.2 p.u.). δ_{vref} is set as 0.5 p.u. to transmit $P =$ 0.5 p.u. to the grid. Low voltage ride through (LVRT) with δ_v-SYN control follows the trajectory delineated by points a, b, c, and d, as depicted in Fig. 7(a). The operating point is at the steady-state equilibrium point a under normal conditions. When V_g suddenly decreases to 62 V (0.2 p.u.), δ will not undergo an abrupt change. Consequently, the operating point will jump to the fault δ_v-δ curve from the standard/post-fault δ_v-δ curve. Because $\delta_{vref} > \delta_v$ at point b on the fault δ_v-δ curve, according to (17), δ will steadily increase and the operating point will move along the fault δ_v-δ curve until it reaches the steady-state equilibrium point c. Then, regardless of the fault duration, the GFMC will consistently operate at point c. When V_g is restored, the operating point will jump from the equilibrium point c to point d. Point d closely ap-

proaches the operating point under normal conditions, making it an advantageous operating point for rapid post-fault resynchronization. δ_v is greater than the reference value δ_{vref} at point d. According to (17), δ_v will decrease and the operating point will move along the post-fault δ_v-δ curve until it reaches point a. Figure 7(b) depicts the variation of active power output with δ during the LVRT process.

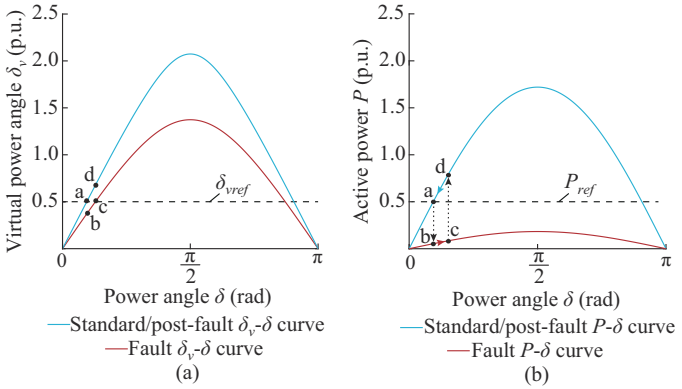

Fig. 7. Operational mechanism of GFMC with δ_v-SYN control under a voltage sag when SCR is 15. (a) δ_v-δ curves. (b) P-δ curves.

The analysis above indicates that after applying the δ_v-SYN control, the GFMC is able to establish a steady-state equilibrium operating point during the voltage sags, regardless of the variation of δ_{vref} ranging from 0 p.u. to 1 p.u.. Consequently, the effectiveness of the control remains unaffected by the extent and duration of the voltage sag under strong grid conditions. Note that once the equilibrium point is reached, the GFMC will stabilize promptly without exhibiting any oscillation.

To analyze the transient stability of δ_v-SYN control under weak grid conditions, Fig. 8 depicts the δ_v-δ curves and P-δ curves of the GFMC under a voltage sag when SCR is 1.5.

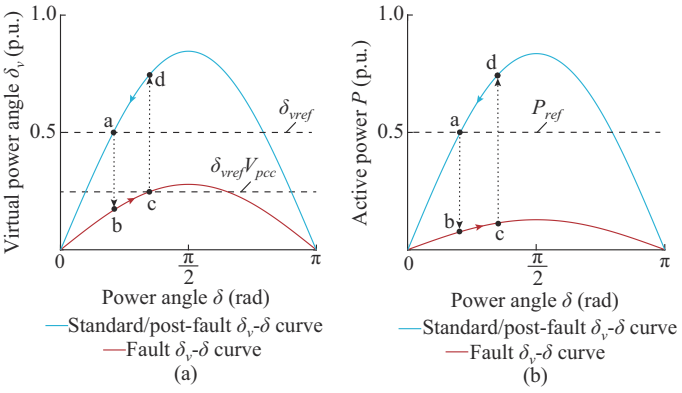

Fig. 8. Operational mechanism of GFMC with δ_v-SYN control under a voltage sag when SCR is 1.5. (a) δ_v-δ curves. (b) P-δ curves.

Figure 8(a) shows that there is no steady-state equilibrium point when a voltage drop occurs. In this scenario, low-frequency oscillations (LFOs) will occur, resulting in transient instability in the system. Therefore, under weak grid conditions, it is essential to adjust δ_{vref} according to the variation of V_{pcc}, e.g., $\delta_{vref}=\delta_{vref}V_{pcc}$, so that the fault δ_v-δ curve intersects with δ_{vref}. The subsequent analysis is similar to the case under strong grid conditions and will not be reiterated.

C. Transient Stability Analysis of δ_v-SYN Control in Case of Frequency Variations

To solve the instability problem of the GFMC with the P-SYN control and the CRS limiting method under frequency variations depicted in Fig. 4, the change of δ can be constrained to prevent δ from reaching point b, which triggers the transition into the CSM.

Since V_g and X_g are typically unidentified, it is challenging to obtain δ. The relationship between the virtual power angle δ_v and the power angle δ is illustrated in Fig. 2. Therefore, restrictions on δ_v can be used to indirectly constrain the variation in δ. Figure 9 shows a block diagram for adding a virtual power angle limit in the δ_v-SYN control. θ'_{ref} represents the phase of the GFMC after adding a virtual power angle limit; and δ_{vlimit} represents the constrained virtual power angle.

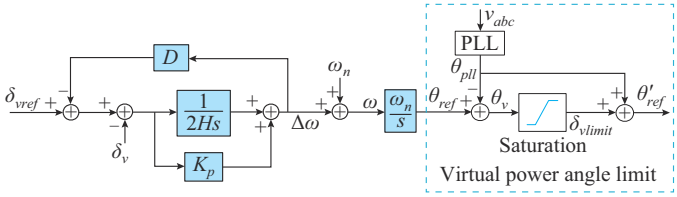

Fig. 9. Control block diagram for adding a virtual power angle limit in δ_v-SYN control.

It is worth noting that the virtual power angle limit only prevents the converter from overcurrent only when the virtual power angle exceeds ±1 p.u.; within the limit range, the virtual power angle limit remains inactive. In Fig. 10, with the grid frequency decreasing from f_1 of 50 Hz to f_2 of 49.6 Hz, the operating point shifts from point a to point c, and δ is restricted to δ_{limit} when the virtual power angle limit is used.

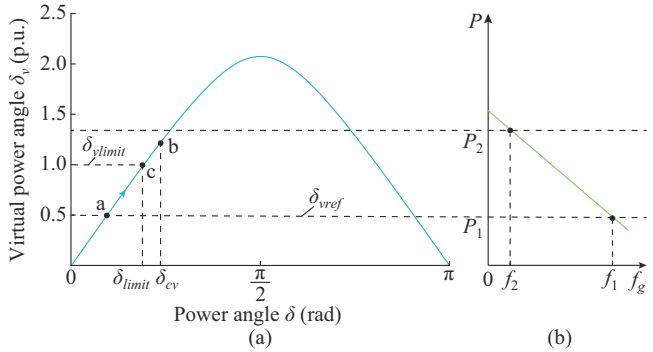

Fig. 10. Theoretical operating trajectories of GFMC with δ_v-SYN control under frequency variations when virtual power angle limit is added. (a) Standard/post-fault δ_v-δ curve. (b) P-f_g curve.

Due to the limitation on δ, δ_{cv} will not be reached. Thus, the transient instability is avoided. It is noteworthy that when the virtual power angle limit is used, the GFMC can generate active power based on its capacity to support the grid frequency under frequency variations.

D. Transient Stability Analysis of δ_v-SYN Control in Case of Phase Jump

Based on the analysis in Section III, when a phase jump of −60° occurs, a loss of synchronization will occur between the grid and the GFMC using the P-SYN control and the CRS limiting method. To analyze the transient stability of the δ_v-SYN control under phase jump, the δ_v-δ curves and P-δ curves of the GFMC are plotted in Fig. 11.

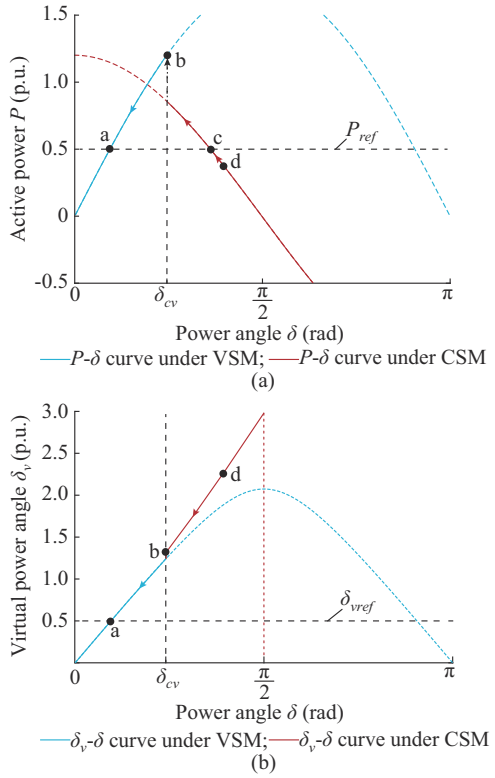

Fig. 11. Theoretical operating trajectories of GFMC with δ_v-SYN control under phase jump. (a) P-δ curves. (b) δ_v-δ curves.

For GFMC with the δ_v-SYN control, a phase jump of −60° will lead to a sudden increase in δ from point a to point d, consequently causing current limiting. According to the δ_v-δ curve, δ_v is greater than the reference value δ_{vref} at point d. Based on (17), δ will decrease and the operating point will move along the δ_v-δ curve under the CSM until it reaches point b, where $\delta = \delta_{cv}$. The CRS limiting method will be deactivated, so the operating point will jump to the δ_v-δ curve under the VSM and trace back along the δ_v-δ curve under the VSM to point a. From the above analysis, it can be concluded that the GFMC with the δ_v-SYN control enhances the transient stability under phase jump compared with the GFMC with the P-SYN control and the CRS limiting method.

V. Case Study

This section evaluates the dynamic performance and robustness of the proposed method under varying grid strengths using time-domain simulations. Additionally, a comparative analysis is presented to highlight the advantages of the proposed method over existing state-of-the-art methods.

A. Dynamic Performance and Robustness Analysis

The proposed method exhibits excellent dynamic response and robustness across varying grid strengths. Figure 12 presents the time-domain simulations for the step response of the active power output of the converter when using the proposed method across various grid strengths.

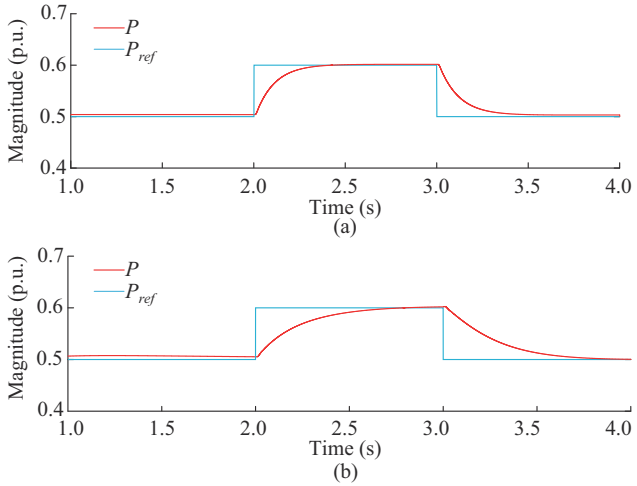

Fig. 12. Step responses of active power output. (a) Under strong grid condition when SCR is 15. (b) Under weak grid condition when SCR is 1.5.

In Fig. 12(a), the active power output of the converter quickly tracks the setpoint when P_{ref} is stepped from 0.5 p.u. to 0.6 p.u. under strong grid conditions when SCR is 15. In Fig. 12(b), the active power output also rapidly tracks the setpoint, demonstrating robust tracking capabilities.

These simulations confirm that the converter with the proposed method achieves excellent dynamic performance and maintains robustness across a wide range of grid strengths.

B. Comparison of Proposed Method with State-of-the-art Methods

To highlight the advantage of the proposed method, a comparison with existing methods for enhancing transient stability is presented. Table I summarizes the pros and cons of six existing methods, evaluated based on seven selected criteria. The SEPFC [19], Q-SYN [20], power angle frequency droop control (PAFDC) [21], and freezing virtual angular speed (FVAS) of grid-forming converter [28] can only improve transient stability in grid voltage sag scenarios. The power-angle-based adaptive overcurrent protection scheme (PAAOPS) [23] can improve transient stability only in grid voltage sag and frequency variation scenarios. The optimal current saturation angle scheme (OCSAS) [22] can address the instability during grid voltage sags and phase jumps by modifying the saturation current phase reference.

To the best of the author's knowledge, existing control methods can only improve transient stability against one or two types of transient disturbances. The main advantage of the proposed method is its ability to improve transient stability of GFMCs under all three common types of transient disturbances.

TABLE I
COMPARISON OF PROS AND CONS OF EXISTING METHODS FOR TRANSIENT STABILITY ENHANCEMENT

Method	Effective to grid voltage sags	Effective to grid frequency drops	Effective to grid phase jumps	Not sensitive to grid impedance or SCR variation	Fast fault current injection	Smooth transition between normal and fault cases	No need for grid impedance detection
SEPFC	√	×	×	×	×	×	√
Q-SYN	√	×	×	×	√	√	×
PAFDC	√	×	×	×	√	√	√
FVAS	√	×	×	×	√	×	√
PAAOPS	√	√	×	×	√	×	√
OCSAS	√	×	√	×	×	×	×
δ_v-SYN	√	√	√	√	√	√	√

A detailed comparison of the proposed method and existing methods under each type of the transient disturbance is provided in Supplementary Material A.

In summary, each of the six existing methods has its inherent disadvantages. In contrast, the proposed method has distinct advantages. It can improve transient stability across all three types of transient disturbances, under both strong and weak grid conditions. It also achieves a seamless transition between normal and fault scenarios. The proposed method does not require online line impedance measurement or fault detection, making it simpler to implement than the existing methods. Additionally, this method can provide fast fault current injection and frequency support during transient disturbances, which will be further validated in the following experiments.

VI. EXPERIMENTAL VALIDATION

As shown in Fig. 13, HIL experiments based on the OPAL-RT platform are conducted to verify the correctness of the theoretical analysis. The power grid and GFMC are simulated using the OPAL-RT platform. The control algorithm is implemented on DSP TMS320F28335. OPAL-RT platform interfaces with the DSP controller through analog output and digital input channels. The parameters of the system are displayed in Table II.

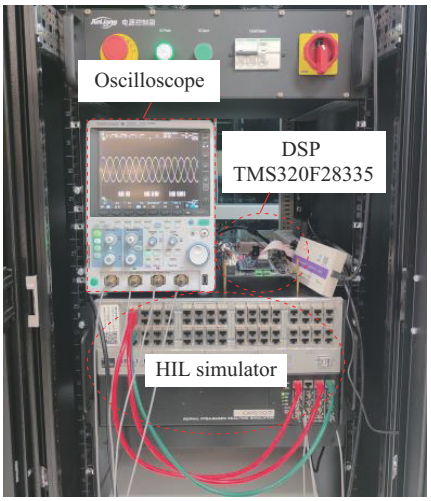

Fig. 13. HIL experiment platform.

TABLE II
PARAMETERS OF SYSTEM

Description	Value
Magnitude of grid voltage V_g (V)	311
Frequency of grid voltage f_g (Hz)	50
Voltage reference V_N (V)	311
The maximum current I_{max} (A)	128 (1.2 p.u.)
Active power reference P_N (kW)	50
DC capacitor voltage V_{dc} (V)	1200
Angular frequency reference ω_N (rad/s)	$2\pi \cdot 50$
Rated apparent power S_N (kVA)	50
Switching frequency f_s (kHz)	10
Filter inductance L_f (H)	0.002
Filter capacitance C_f (F)	2×10^{-5}
Virtual resistance R_v (p.u.)	0.08
Virtual inductance L_v (p.u.)	0.8
SCR	1.5-15
Line inductance L_g (mH)	0.6-6
Droop parameter D (p.u.)	100
Proportional gain of APC K_p (p.u.)	0.001
Inertial constant H (p.u.)	5
Reactive power droop coefficient n_q	$10\% \cdot V_N/P_N$
Proportional coefficient of CLC K_{pi}	2.5
Integral coefficient of CLC K_{ii}	10
Cutoff frequency of LPFs f_{LPF} (Hz)	10
Proportional coefficient of PLL K_{ppll}	0.128
Integral coefficient of PLL K_{ipll}	1.28

In order to validate the transient stability issues identified from the P-δ curves, experiments were conducted using the system and control illustrated in Fig. 1. As illustrated in Fig. 14(a), the disturbance is emulated by abruptly transitioning V_g from 311 V (1 p.u.) to 62 V (0.2 p.u.) and lasts for 1 s. The CRS limiting method restricts the converter current, i_L = 1.2 p.u.. The voltage sag and current limitation cause a reduction in P. Since $P<P_{ref}$, based on (6), δ will increase. When δ exceeds the critical threshold δ_d described in Fig. 3, the system becomes unstable. Then δ keeps increasing rapidly, eventually leading to the desynchronization of the GFMC

from the grid. Therefore, the P-SYN control with the CRS limiting method fails to ensure the transient stability of the converter during grid voltage sags. The experiment aligns with the theoretical analysis. In Fig. 14, V_a is the one-phase output voltage of the converter; i_{La} is the converter-side one-phase current; and Q is the reactive power output of the converter.

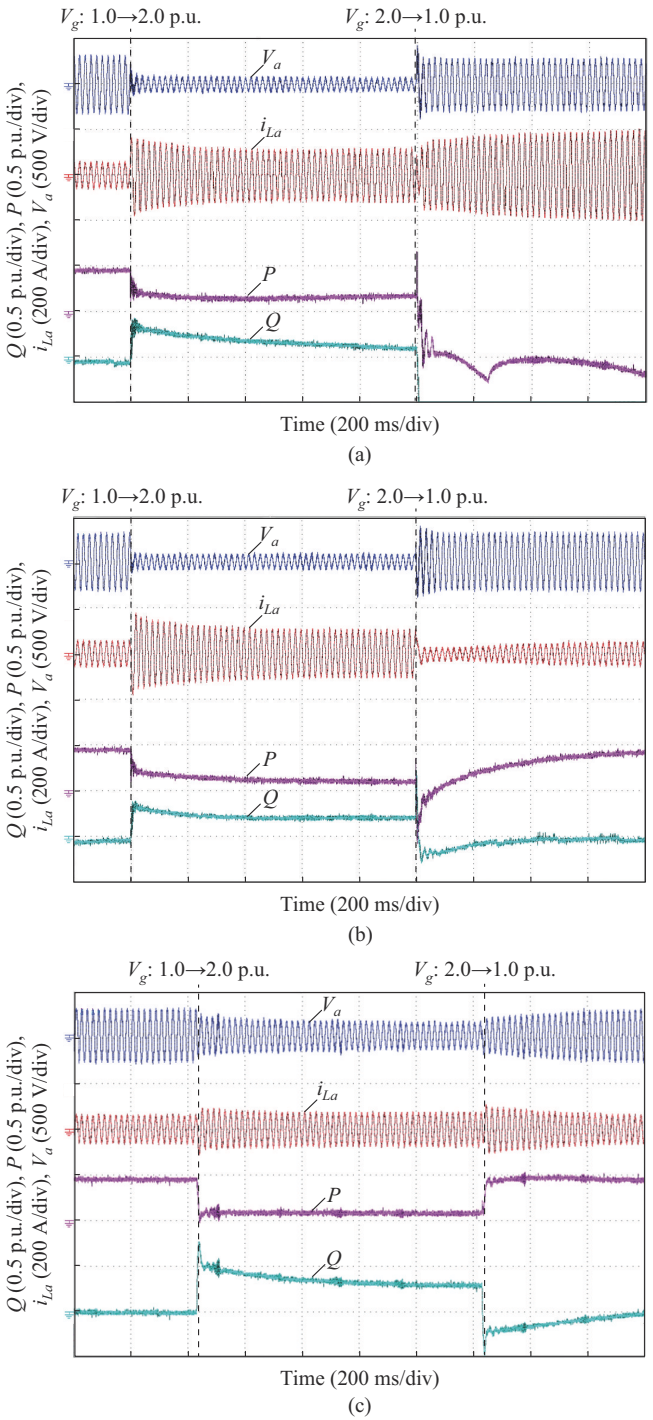

Fig. 14. Experiment results in grid voltage sag scenarios. (a) P-SYN control with CRS limiting method. (b) Proposed method when SCR is 15. (c) Proposed method when SCR is 1.5.

The experiments of the proposed method in grid voltage sag scenarios are depicted in Fig. 14(b) and Fig. 14(c), wherein V_g decreases from 311 V (1 p.u.) to 62 V (0.2 p.u.) and lasts for 1 s. During a voltage sag, V_a, i_{La}, and output power remain stable. This indicates that the converter maintains synchronization with the grid during the disturbance regardless of the fault duration. During the fault, the proposed method effectively constrains the current magnitude within 1.2 p.u..

Furthermore, the GFMC provides 0.4 p.u. of reactive power when SCR is 15 and 0.5 p. u. of reactive power when SCR is 1.5 to support grid voltage during the voltage sag. Once the fault is cleared, the GFMC successfully returns to its pre-fault state. The proposed method inherently guarantees the existence of the equilibrium point of the GFMC during the voltage sag, thereby preventing transient instability of the GFMC, as discussed in Section III.

The experiment results in frequency variation scenarios are depicted in Fig. 15. The power reference is initially set to be 0.5 p.u.. The frequency variation occurs and lasts for 0.6 s. Figure 15(a) illustrates the response of the P-SYN control with the CRS limiting method. Upon the decrease of the grid frequency from 50 to 49.6 Hz, δ will swing past the unstable equilibrium point during the fault described in Fig. 4. The output power becomes unstable, and the output current becomes saturated. This result is consistent with the theoretical observations depicted in Fig. 4. Conversely, as illustrated in Fig. 15(b), employing the proposed method results in stable restriction of the current within the rated value. Meanwhile, when the grid frequency decreases, the converter outputs more active power to support the grid frequency. Additionally, to evaluate the efficiency of the proposed method under weak grid conditions when SCR is 1.5, a further experiment is conducted as in Fig. 15(c). The power output of the converter is limited under weak grid conditions. Therefore, when the grid frequency decreases, the converter will not enter CSM, preventing transient instability.

Figure 16 presents the experiment results of the P-SYN control with the CRS limiting method and the proposed method in phase jump scenarios. Figure 16(a) demonstrates the dynamic reactions of the P-SYN control with the CRS limiting method under the strong grid condition when SCR is 15. When a phase jump of −60° occurs, δ crosses the unstable equilibrium point. The fluctuations in the output power are evident, indicating that the GFMC loses synchronization with the grid. The experiment result is consistent with the theoretical observations depicted in Fig. 5. Conversely, as depicted in Fig. 16(b), the proposed method makes it possible to maintain the grid synchronization even during a phase jump of −60°. After the disturbance, the operating point can return to its pre-fault state. Due to the fact that the voltage and current do not perfectly track the reference values in the dynamic process, the output current slightly exceeds 1.2 p.u.. Our future research will focus on eliminating this slight overcurrent. As illustrated in Fig. 16(c), the proposed method can also maintain synchronization with the grid during a phase jump of −60° under weak grid conditions.

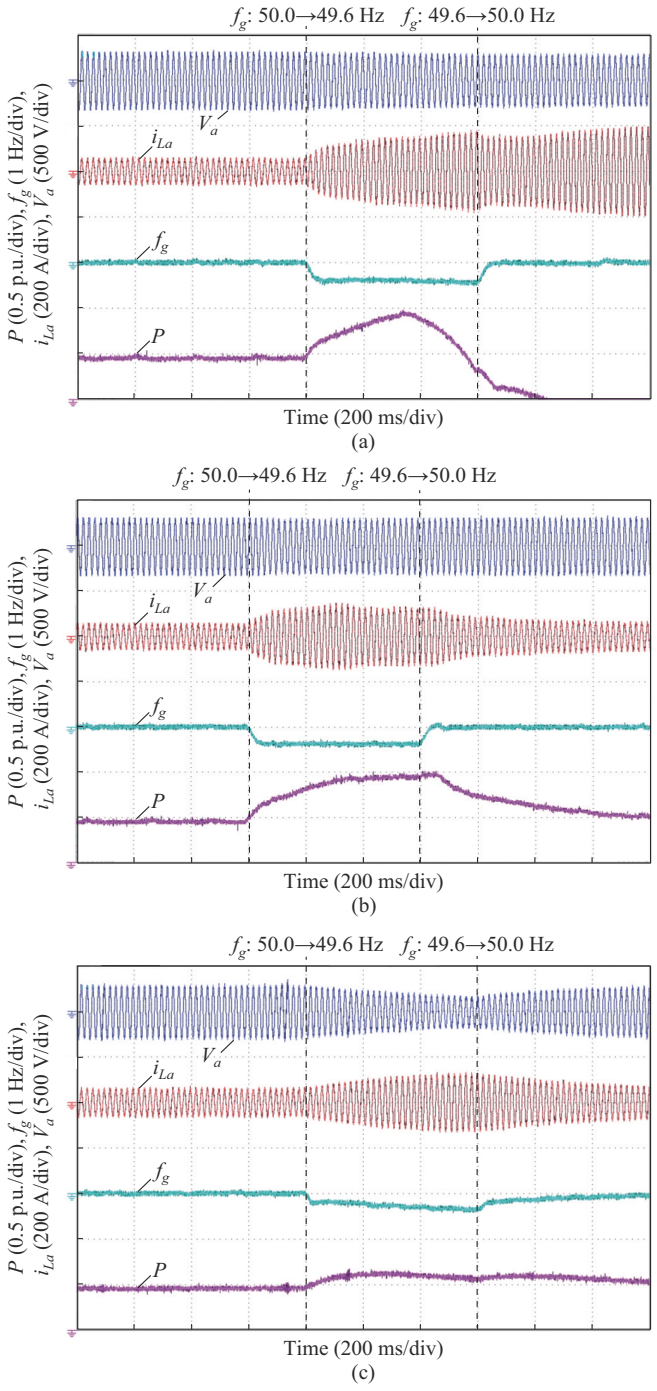

Fig. 15. Experiment results in frequency variation scenarios. (a) P-SYN control with CRS limiting method when SCR is 15. (b) Proposed method when SCR is 15. (c) Proposed method when SCR is 1.5.

VII. Conclusion

This study first analyzes the instability mechanisms of GFMCs with the P-SYN control and the CRS limiting method under various transient disturbances. Then, a robust δ_v-SYN control method for GFMCs is proposed. It can guarantee the presence of a steady-state equilibrium point during transient disturbances, thus ensuring transient stability during voltage sags, frequency variations, and phase jumps in both strong and weak grids. Additionally, the GFMC with the δ_v-SYN control can offer support for the voltage and frequency of the grid during disturbances. Ultimately, experimental findings confirm the correctness of the theoretical analysis and the efficacy of the proposed method. In future work, further investigation into the transient stability of multiple converter systems will be conducted.

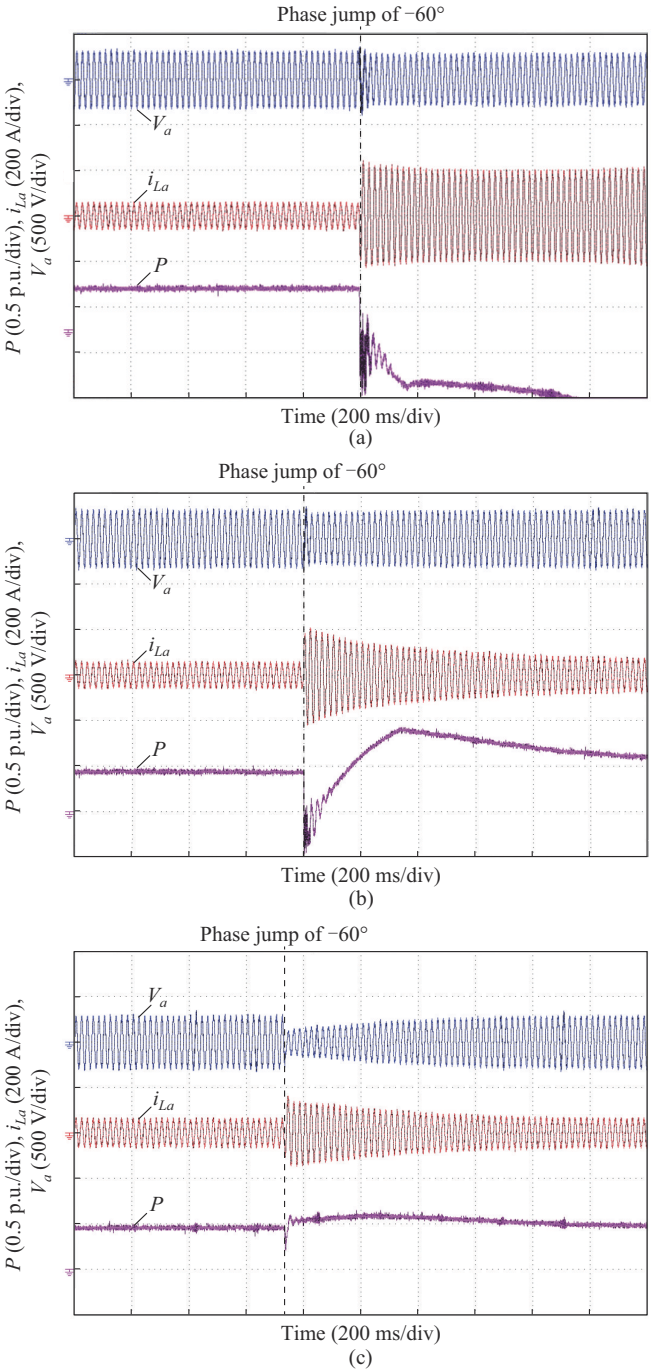

Fig. 16. Experiment results in phase jump scenarios. (a) P-SYN control with CRS limiting method during a phase jump of −60° when SCR is 15. (b) Proposed method during a phase jump of −60° when SCR is 15. (c) Proposed method during a phase jump of −60° when SCR is 1.5.

References

[1] J. Feng, W. Xiang, J. Wen *et al.*, "Mid- and high-frequency resonance characteristics and suppression strategies of VSC-UHVDC for large-

scale renewable energy transmission," *Journal of Modern Power Systems and Clean Energy*, vol. 12, no. 6, pp. 2058-2070, Nov. 2024.
[2] R. H. Lasseter, Z. Chen, and D. Pattabiraman, "Grid-forming inverters: a critical asset for the power grid," *IEEE Journal of Emerging and Selected Topics in Power Electronics*, vol. 8, no. 2, pp. 925-935, Jun. 2020.
[3] L. Zhang, L. Harnefors, and H. P. Nee, "Power-synchronization control of grid-connected voltage-source converters," *IEEE Transactions on Power Systems*, vol. 25, no. 2, pp. 809-820, May 2010.
[4] L. Harnefors, F. M. M. Rahman, M. Hinkkanen *et al*., "Reference-feedforward power-synchronization control," *IEEE Transactions on Power Electronics*, vol. 35, no. 9, pp. 8878-8881, Sept. 2020.
[5] L. Harnefors, M. Hinkkanen, U. Riaz *et al*., "Robust analytic design of power-synchronization control," *IEEE Transactions on Industrial Electronics*, vol. 66, no. 8, pp. 5810-5819, Aug. 2019.
[6] H. Wu and X. Wang, "Design-oriented transient stability analysis of grid-connected converters with power synchronization control," *IEEE Transactions on Industrial Electronics*, vol. 66, no. 8, pp. 6473-6482, Aug. 2019.
[7] D. Pan, X. Wang, F. Liu *et al*., "Transient stability of voltage-source converters with grid-forming control: a design-oriented study," *IEEE Journal of Emerging and Selected Topics in Power Electronics*, vol. 8, no. 2, pp. 1019-1033, Jun. 2020.
[8] X. Xiong, C. Wu, and F. Blaabjerg, "Effects of virtual resistance on transient stability of virtual synchronous generators under grid voltage sag," *IEEE Transactions on Industrial Electronics*, vol. 69, no. 5, pp. 4754-4764, May 2022.
[9] M. Chen, D. Zhou, and F. Blaabjerg, "Enhanced transient angle stability control of grid-forming converter based on virtual synchronous generator," *IEEE Transactions on Industrial Electronics*, vol. 69, no. 9, pp. 9133-9144, Sept. 2022.
[10] H. Wu and X. Wang, "A mode-adaptive power-angle control method for transient stability enhancement of virtual synchronous generators," *IEEE Journal of Emerging and Selected Topics in Power Electronics*, vol. 8, no. 2, pp. 1034-1049, Jun. 2020.
[11] H. Xin, L. Huang, L. Zhang *et al*., "Synchronous instability mechanism of *P-f* droop-controlled voltage source converter caused by current saturation," *IEEE Transactions on Power Systems*, vol. 31, no. 6, pp. 5206-5207, Nov. 2016.
[12] K. O. Oureilidis and C. S. Demoulias, "A fault clearing method in converter-dominated microgrids with conventional protection means," *IEEE Transactions on Power Electronics*, vol. 31, no. 6, pp. 4628-4640, Jun. 2016.
[13] M. G. Taul, X. Wang, P. Davari *et al*., "Current limiting control with enhanced dynamics of grid-forming converters during fault conditions," *IEEE Journal of Emerging and Selected Topics in Power Electronics*, vol. 8, no. 2, pp. 1062-1073, Jun. 2020.
[14] I. Sadeghkhani, M. E. H. Golshan, J. M. Guerrero *et al*., "A current limiting strategy to improve fault ride-through of inverter interfaced autonomous microgrids," *IEEE Transactions on Smart Grid*, vol. 8, no. 5, pp. 2138-2148, Sept. 2017.
[15] X. Lin, Z. Liang, Y. Zheng *et al*., "A current limiting strategy with parallel virtual impedance for three-phase three-leg inverter under asymmetrical short-circuit fault to improve the controllable capability of fault currents," *IEEE Transactions on Power Electronics*, vol. 34, no. 8, pp. 8138-8149, Aug. 2019.
[16] R. Rosso, S. Engelken, and M. Liserre, "On the implementation of an FRT strategy for grid-forming converters under symmetrical and asymmetrical grid faults," *IEEE Transactions on Industry Applications*, vol. 57, no. 5, pp. 4385-4397, Sept. 2021.
[17] A. D. Paquette and D. M. Divan, "Virtual impedance current limiting for inverters in microgrids with synchronous generators," *IEEE Transactions on Industry Applications*, vol. 51, no. 2, pp. 1630-1638, Mar. 2015.
[18] T. Qoria, F. Gruson, F. Colas *et al*., "Current limiting algorithms and transient stability analysis of grid-forming VSCs," *Electric Power Systems Research*, vol. 189, p. 106726, Dec. 2020.
[19] L. Huang, H. Xin, Z. Wang *et al*., "Transient stability analysis and control design of droop-controlled voltage source converters considering current limitation," *IEEE Transactions on Smart Grid*, vol. 10, no. 1, pp. 578-591, Jan. 2019.
[20] H. Deng, Y. Qi, J. Fang *et al*., "A robust low-voltage-ride-through strategy for grid-forming converters based on reactive power synchronization," *IEEE Transactions on Power Electronics*, vol. 38, no. 1, pp. 346-357, Jan. 2023.
[21] J. Erdocia, A. Urtasun, and L. Marroyo, "Power angle-frequency droop control to enhance transient stability of grid-forming inverters under voltage dips," *IEEE Journal of Emerging and Selected Topics in Power Electronics*, vol. 11, no. 4, pp. 3751-3764, Aug. 2023.
[22] E. Rokrok, T. Qoria, A. Bruyere *et al*., "Transient stability assessment and enhancement of grid-forming converters embedding current reference saturation as current limiting strategy," *IEEE Transactions on Power Systems*, vol. 37, no. 2, pp. 1519-1531, Mar. 2022.
[23] L. Huang, C. Wu, D. Zhou *et al*., "A power-angle-based adaptive overcurrent protection scheme for grid-forming inverter under large grid disturbances," *IEEE Transactions on Industrial Electronics*, vol. 70, no. 6, pp. 5927-5936, Jun. 2023.
[24] W. Zhang, A. Tarraso, J. Rocabert *et al*., "Frequency support properties of the synchronous power control for grid-connected converters," *IEEE Transactions on Industry Applications*, vol. 55, no. 5, pp. 5178-5189, Sept. 2019.
[25] T. Wen, X. Zou, D. Zhu *et al*., "Comprehensive perspective on virtual inductor for improved power decoupling of virtual synchronous generator control," *IET Renewable Power Generation*, vol. 14, no. 4, pp. 485-494, Mar. 2020.
[26] H. Yuan, X. Yuan, and J. Hu, "Modeling of grid-connected VSCs for power system small-signal stability analysis in DC-link voltage control timescale," *IEEE Transactions on Power Systems*, vol. 32, no. 5, pp. 3981-3991, Sept. 2017.
[27] L. Huang, C. Wu, D. Zhou *et al*., "Impact of virtual admittance on small-signal stability of grid-forming inverters," in *Proceedings of 2021 6th IEEE Workshop on the Electronic Grid*, New Orleans, USA, Nov. 2021, pp. 1-8.
[28] X. Zhao and D. Flynn, "Freezing grid-forming converter virtual angular speed to enhance transient stability under current reference limiting," in *Proceedings of 2020 IEEE 21st Workshop on Control and Modeling for Power Electronics*, Aalborg, Denmark, Nov. 2020, pp. 1-7.

Jidong Xu received the B.S. degree in electrical engineering and automation from China University of Mining and Technology, Xuzhou, China, in 2022. He is currently pursuing an M.S. degree in electrical engineering at South China University of Technology, Guangzhou, China. His research interests include transient stability analysis and enhancement of grid-forming converters.

Jun Zeng received the Ph.D. degree in control theory and control engineering from South China University of Technology, Guangzhou, China, in 2007. She is currently a Professor at the School of Electrical Power Engineering, South China University of Technology. Her current research interests include power electronics applications, energy management, and intelligence control in distributed generation and integration of renewable energy to smart grids.

Gengning Ying received the B.S. degree from Jiangnan University, Wuxi, China, in 2020. He is presently working towards the Ph.D. degree in electrical engineering at the School of Electric Power Engineering, South China University of Technology, Guangzhou, China. His research interests include power electronic application, modeling and control of grid-connected converter, and stability analysis of renewable energy generation system.

Minhai Wu received the B.S. degree from Jiangnan University, Wuxi, China and the M.S. degree in electrical engineering from the School of Electric Power Engineering, South China University of Technology, Guangzhou, China, in 2021 and 2024, respectively. He is now working in the State Grid Anhui Wuhu Power Supply Company, Wuhu, China. His research interests include modeling and control of grid-connected converter and stability analysis of renewable energy generation system.

Junfeng Liu received the M.S. degree in control engineering from South China University of Technology, Guangzhou, China, in 2005, and the Ph.D. degree from the Hong Kong Polytechnic University, Hong Kong, China, in 2013. From 2005 to 2008, he was a Development Engineer with the GSM/UMTS Department in Guangdong Nortel Network, Guangzhou, China. In 2014, he joined the South China University of Technology, where he is currently a Professor at the School of Automation Science and Engineering. His research interests include power electronics application, nonlinear control, high-frequency power distribution system, and motion control system.